Magnetic Resonance in Medicine 59:764–770 (2008)

Visualization of the Coherence of the Principal Diffusion Orientation: An Eigenvector-Based Approach

JiunJie Wang,[1,2] YuChun Lin,[1,2] YauYau Wai,[1,2] HaoLi Liu,[3] ChingPo Lin,[4] and YingZu Huang[5*]

A novel method for spatially mapping anisotropy/orientation coherence of the eigenvector is presented. By using an eigenvector-based approach, an intervoxel diffusion coherence (IVDC) index was used to quantify the coherence of the principal diffusion directions within a voxel neighborhood. This method may allow reconstruction of a whole brain map to be used for diagnostic purposes. The IVDC index is calculated by a scatter matrix-based method in a voxel-wise manner. A simulation was performed using two fiber populations crossing at various separation angles. We demonstrate that the IVDC index was more sensitive than fractional anisotropy (FA) to changes in separation between the fibers under a noise-free condition. Diffusion-tensor images of six healthy volunteers were acquired on a 3.0T MR imager. The FA, coherence index, and IVDC were then calculated. The results showed that IVDC improved the contrast in several brain areas including thalamus, middle cerebral peduncle, and pons. We therefore conclude that the IVDC index provides reliable and complementary information on water diffusion in the brain. It may be useful in white matter tractography, especially to determine the termination point of a trajectory. Magn Reson Med 59:764–770, 2008. © 2008 Wiley-Liss, Inc.

Key words: DTI; eigenvector; diffusion anisotropy; scatter matrix

Growing evidence has suggested that diffusion-tensor imaging (DTI) may be clinically useful in many brain diseases including multiple sclerosis and head trauma (1–5). The measured diffusion tensor may be used to provide information about the integrity, location, and orientation of white matter tracts in the brain. The eigenvalues indicate the magnitude of the diffusion along the directions pointed by the eigenvectors. The diffusion tensor contains information related to the diffusion anisotropy and mean diffusivity.

Several diffusion anisotropy indices have been calculated from the eigenvalues, including relative anisotropy (RA) (6), ultimate anisotropy (7), and volume ratio (8). Fractional anisotropy (FA) is one of the most frequently used (6) because of its good sensitivity and tolerance to noise (9–12). By preference, the index should be rotationally invariant and scaled between 0 and 1. However, current indices do not provide information on microstructure orientation.

Diffusion anisotropy indices are often based on intravoxel effects caused by biophysical tissue properties. They provide information on the relationship between the eigenvalues within a voxel-of-interest (13). Notably, current anisotropy indices rarely provide information about the diffusion of water among neighboring voxels. Klingberg et al. (14) previously proposed the use of the coherence index (CI) as a measure of diffusion anisotropy. The CI in a voxel is defined as the mean cosine for the angle between the principal diffusion directions of the voxel and its eight neighbors. By using this index the authors demonstrated that the right frontal lobe has a more regular organization of axons compared to the left in both children and adults.

Basser et al. (13) previously introduced a positive semidefinite second-order dyadic tensor to describe the angular uniformity of the eigenvector distribution of the diffusion tensor within a region of interest (ROI) (15). Wu et al. (16) further used the dyadic matrix of the major eigenvectors, termed *raT*, to describe the directional coherence of the principal water diffusion in a selected ROI. The use of *raT* allowed objective analysis of the anisotropic diffusion within tissue that previously relied on subjective assessments of directional color-encoded maps. Unfortunately, this analysis is limited to preselected regions and fails to produce maps showing the directional distribution that may eventually have diagnostic importance.

In the present study we propose a new method for spatially mapping the coherence of the eigenvector orientation, termed intervoxel diffusion coherence (IVDC). The IVDC may be conceptualized as a further development of *raT*. Specifically, it is an eigenvector-based analysis that provides information on the anisotropic diffusion among voxels. With the use of this index, a whole brain map can be reconstructed.

MATERIALS AND METHODS

InterVoxel Diffusion Coherence Index

The diffusion tensor $\mathbf{D}$ can be described by a 3×3 symmetric matrix as shown in Eq. [1], where $\mathbf{D}_{ij}$ indicates the diffusion coefficient reflecting the correlation of the diffusional flux in the i direction with the concentration gradient in the j direction.

[1]Department of Medical Imaging and Radiological Sciences, Chang Gung University, Taiwan.

[2]Magnetic Resonance Imaging Centre, Chang Gung Memorial Hospital, Taiwan.

[3]Department of Electrical Engineering, Chang Gung University, Taiwan.

[4]Institute of Neuroscience, National Yang-Ming University, Taiwan.

[5]Department of Neurology, Chang Gung Memorial Hospital, Taiwan.

Grant sponsor: National Science Council, Taiwan; Grant number: NSC-95-2614-B-182-002; Grant sponsor: Molecular Imaging Centre, ChangGung Memorial Hospital Medical Research Project; Grant number: CMRP34009.

*Correspondence to: YingZu Huang, Department of Neurology, Chang Gung Memorial Hospital, Taiwan. E-mail: jwang@mail.cgu.edu.tw

Received 6 March 2007; revised 26 September 2007; accepted 1 October 2007.

DOI 10.1002/mrm.21458
Published online in Wiley InterScience (www.interscience.wiley.com).

$$D = \begin{bmatrix} D_{xx} & D_{xy} & D_{xz} \\ D_{yx} & D_{yy} & D_{yz} \\ D_{zx} & D_{zy} & D_{zz} \end{bmatrix} \quad [1]$$

The scatter matrix **T** is a symmetric, positive, and semidefinite second-order dyadic tensor of size 3 × 3 as described by Wu et al. (16). It is defined as:

$$\mathrm{T} = \frac{1}{n}\sum_{i=1}^{n} \varepsilon_{\mathrm{li}} \varepsilon_{\mathrm{li}}' \quad [2]$$

Each element in the scatter matrix contains products of the *x*, *y*, and *z* components of the principal eigenvector ε_{1i}, where ε_{1i} indicates the major eigenvector of the ith voxel.

The angular uniformity of the eigenvector distribution within the ROI may be described using the parameter, *raT*, which quantifies the anisotropy of the scatter matrix **T** in a manner analogous to RA as in Eq [3]:

$$raT = \frac{\sqrt{(t_1 - \bar{t})^2 + (t_2 - \bar{t})^2 + (t_3 - \bar{t})^2}}{\sqrt{6}t} \quad [3]$$

Where the parameters *t* with subscript are the eigenvalues of the scatter matrix. The parameter $\bar{t}$ is the mean eigenvalue, which is equal to one-third since the major eigenvectors are unit vectors.

The parameter *raT* is normalized between 0 (complete isotropy) and 1 (complete anisotropy). Regions with highly coherent or collinear eigenvector organization have a large value of *raT*. Regions with small *raT* denote an either random or noncollinear eigenvector distribution. The value of *raT* is influenced by both the size of ROI and the intrinsic distribution of eigenvectors.

The IVDC is an extension of *raT*. The IVDC at a specific voxel represents a localized *raT*. A local scatter matrix **T′** is defined on the basis of a local ROI consisting of the 26 nearest-neighboring voxels. The IVDC is then computed in a manner analogous to *raT*, as in Eq. [4]:

$$IVDC = \frac{\sqrt{(t_1' - \bar{t}')^2 + (t_2' - \bar{t}')^2 + (t_3' - \bar{t}')^2}}{\sqrt{6}t'} = \sqrt{\frac{3}{2}} * \sqrt{(t_1' - \bar{t}')^2 + (t_2' - \bar{t}')^2 + (t_3' - \bar{t}')^2} \quad [4]$$

where the parameters t' with subscript represent the eigenvalues of the scatter matrix **T′**, and $\bar{t}'$ is the mean eigenvalue.

IVDC maps of the whole brain can be generated by performing the computation in each voxel. IVDC may be computed with ROIs of different sizes. In the current study the computations were performed using an ROI of the 26 nearest-neighboring voxels in 3D space. A high IVDC indicates a highly coherent eigenvector organization between the voxel of interest (VOI) and its neighborhood. It provides a quantitative measurement of the directional coherence of the principal water diffusion.

For comparison, both FA and CI were calculated by Eqs. [5] and [6], respectively. $\lambda_{1,2,3}$ indicate the eigenvalues of the diffusion tensor from Eq. [1], whereas $\bar{\lambda}$ denotes the mean eigenvalue.

$$FA = \sqrt{\frac{3}{2}} * \sqrt{\frac{(\lambda_1 - \bar{\lambda})^2 + (\lambda_2 - \bar{\lambda})^2 + (\lambda_3 - \bar{\lambda})^2}{\lambda_1^2 + \lambda_2^2 + \lambda_3^2}} \quad [5]$$

$$Cl_{ij} = \frac{1}{8}\left(\sum_{r=i-1}^{i+1}\sum_{c=j-1}^{j+1} \varepsilon_{ij} \cdot \varepsilon_{rc} - 1\right) \quad [6]$$

The principal eigenvector ε with subscript *i* and *j* defines the main diffusion direction in the voxel at (*i*, *j*) in 2D space. The CI represents the mean dot product of the primary eigenvector in the voxel at (*i*, *j*) and the primary eigenvectors in its eight nearest neighbors.

Simulation Studies

In a manner similar to the work by Tournier et al. (17), the simulations were performed by assuming the presence of two separate fiber populations in two neighboring voxels. The fibers travel in parallel from a beginning point. After reaching a separation point, the first fiber population continues moving in the same direction, while the direction of the second population in the neighboring voxel is rotated to a separation angle θ_{sep}. Simulations were performed for separation angles ranging from 0–90°. For each simulation the separation angle was incremented by an additional 5°. The simulation was performed under two different conditions: 1) constant eigenvalues for eigenvectors rotation, and 2) the presence of fibers in neighboring voxels only.

The diffusion-weighted signal attenuation was calculated assuming a prolate tensor model ($\lambda_1 = 10 \times (\lambda_2 = \lambda_3)$, where $\lambda_{1,2,3}$ indicate the eigenvalues of the diffusion tensor). It leads to an equal FA of 0.89 for both fibers. The signal was then sampled for a set of noncollinear diffusion weighting gradient orientations. The diffusion weighting gradient was applied using four different combinations of 6, 12, and 25 different directions, respectively. The first and second combination, expressed in terms of (x,y,z), were (−1,1,0), (−1,0,1), (1,1,0), (1,0,1), (0,−1,1), (0,1,1) and (1,0,0), (0,1,0), (0,0,1), (1,1,0), (1,0,1), (0,1,1), respectively. The third and fourth dataset (in 12 directions and 25 directions, respectively) were calculated using the electrostatic repulsion model (18).

To closely mimic the in vivo conditions, the synthetic tensors were constructed to have a trace of 2.1×10^{-5} mm²/s, comparable to that in normal brain parenchyma. Diffusion weighting was simulated with a *b*-value of 1000 s/mm². Maps of FA, CI, and IVDC were computed for the entire phantom. The value from the voxel of the second fiber after rotation was then recorded.

DTI Measurements

This study was approved by our Institutional Review Board. We enrolled a total of six healthy subjects (mean age: 27.3 ± 8.0 years). DTI data were acquired on a 3.0T MR scanner (Magnetom Trio with TIM, Siemens, Erlangen, Germany) using a single-shot spin-echo echo-planar imaging sequence. Acquisition parameters were: TR/TE = 7300/87 ms and *b*-value = 1000 s/mm². The field of view

was 192 mm with a matrix size of 128 × 128. The diffusion weighting gradients were applied in 12 noncollinear directions, as in the third dataset in the simulation. For each direction 56 contiguous axial slices (2-mm thickness) were obtained. Six averages were measured for a total acquisition time of 9 min, 53 sec. For anatomical reference, a T_1-weighted MPRAGE sequence was acquired in all subjects. The imaging parameters were TR/TE/flip angle = 2000 ms/4.16 ms/9°. One hundred sixty sagittal slices covering the whole brain were acquired in 9 min, 14 sec, with an isotropic spatial resolution of 1 mm^3.

Data Analysis

All data postprocessing was performed with MatLab 7.0 (MathWorks, Natick, MA). The map of IVDC was reconstructed in a voxel-by-voxel manner. For comparison purposes, the maps of CI, FA, and color-encoded FA were calculated. Color-encoded FA maps of the corresponding slices were calculated using Dtistudio (v. 2.4; Johns Hopkins University, Baltimore, MD) (19). ROIs were drawn in eight different areas, including the superior longitudinal fasciculus (SLF), corona radiata (CR), corpus callosum (CC), external capsule (EC), posterior limb of internal capsule (PLIC), thalamus, splenium, and lentiform nucleus (LN).

RESULTS

Figure 1 plots the results of simulation studies. The values of FA (solid), CI (in star, diamond, circle, and square for diffusion-encoding schemes along four different directions, respectively), and IVDC (dashed) at the fiber separation point were plotted against the angle of separation (incremented at 5° a step from 0 to 90°). FA remained constant (0.89) throughout the range of simulation since

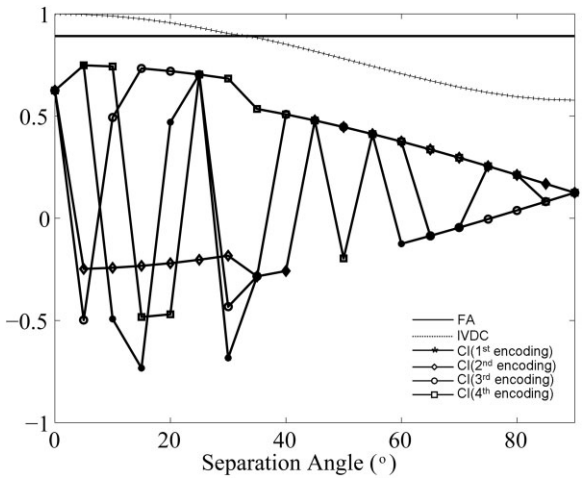

FIG. 1. Diffusion anisotropy indices at fiber crossover locations, plotted against the separation angle. The values of FA (solid), IVDC (dashed), and CI (star for the first diffusion encoding of six directions, diamond for the second diffusion encoding of six directions, circle for the third diffusion encoding of 12 directions, and square for fourth diffusion encoding of 25 directions, respectively) at the points of fiber separation are plotted against the separation angle. The separation angle was incremented by 5° intervals from 0 to 90°.

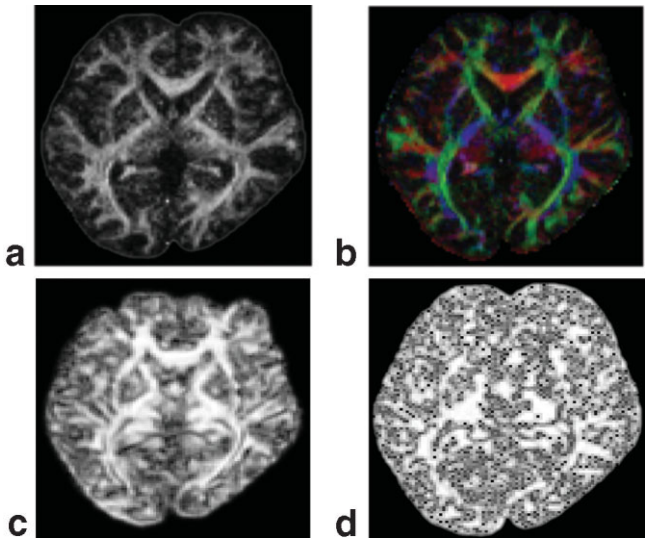

FIG. 2. Images of the calculated indices at the basal ganglia from a healthy subject. **(a)** Fractional Anisotropy (FA), **(b)** color-encoded FA, **(c)** InterVoxel Diffusion Coherence (IVDC), and **(d)** Coherence Index.

the eigenvalues of the diffusion tensor did not change following fiber separation. CI provided a simple average of the cosine angles among the voxels within the ROI, varying over a wide interval in an apparently random manner. It was easily affected by diffusion encoding schemes. On the other hand, IVDC decreased monotonously from a maximum of 1 at 0° to a minimum of 0.58 at 90°, regardless of the diffusion encoding scheme used.

Figure 2 shows transaxial maps of the calculated indices through the brain of one of the normal subjects at the level of the basal ganglia. FA is displayed in both grayscale (Fig. 2a) and with color encoding (Fig. 2b). Corresponding images of IVDC and CI are provided in Fig. 2c,d, respectively. Similar contrast is evident in the IVDC and FA maps, with both showing high values in the white matter and low in the cerebrospinal fluid and gray matter. The CI map is relatively noisy and poorly delineates the boundaries of the soft tissue components. Values of FA and IVDC from selected brain regions are plotted in Fig. 3. The values of *raT*, quoted from Wu et al., were included for comparison.

Figure 4 shows the principal eigenvector of the diffusion tensor projected onto the x-y plane for each voxel within a selected ROI. Arrows representing the projected eigenvectors are superimposed onto the corresponding maps of FA and IVDC. The ROI was selected in the region of the left thalamus as indicated in the T_2-weighted image from one of the volunteers (Fig. 4a). The IVDC map shows homogeneously increased values at sites where the directions of the projected principal diffusion tensor eigenvectors are locally uniform. In contrast, decreased values are evident in the corresponding FA map.

Figure 5 shows transaxial images at the level of the middle cerebellar peduncles and pons. The corresponding FA and IVDC maps are shown in Fig. 5a,b, respectively. Figure 5c is a T_1-weighted image from a nearby slice. Figure 5d represents the corresponding T_2-weighted image. The arrow indicates a ring-like region of low IVDC in

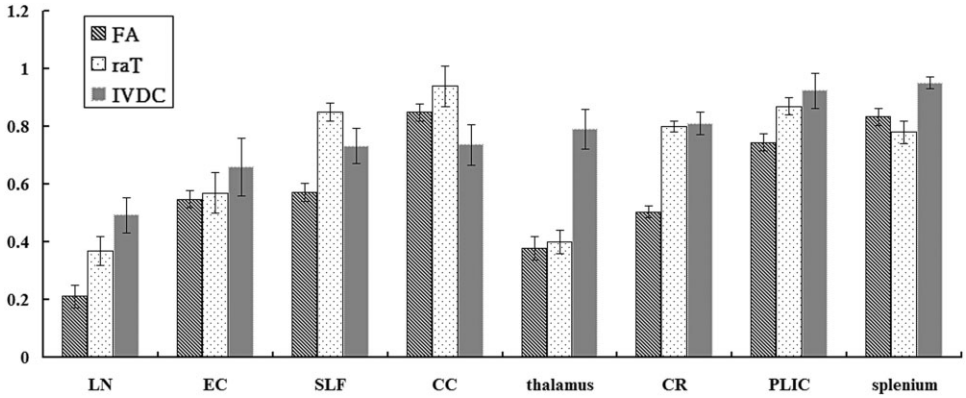

FIG. 3. Mean values of the diffusion anisotropy indices averaged across all subjects. ROIs were selected in the lentiform nucleus (LN), external capsule (EC), superior longitudinal fasciculus (SLF), body of the corpus callosum (CC), corona radiata (CR), and posterior limb of the internal capsule (PLIC). The values of *raT* were drawn from Wu et al. (16).

each side of the pons, possibly providing improved structural delineation as will be discussed later in more detail.

Figure 6 shows the IVDC maps derived from a different volunteer using different sizes of local neighborhoods. Four different sizes of ROI were used. Distances from the original VOI were (3,3,1), (5,5,1), (3,3,3), and (5,5,5), respectively (Fig. 6a–d). The first two ROIs measured in-plane diffusion only. Other ROIs were computed in a 3D space. Maps derived from masks of (5,5,1) and (3,3,3) had a similar ROI size (26 voxels and 24 voxels, respectively).

DISCUSSION

Comparison of the Diffusion Anisotropy Indices

The extent of the water diffusion anisotropy involves at least two aspects: the deviation among the eigenvalues within a VOI and the direction coherence of the water diffusion in an ROI. Accordingly, the diffusion anisotropy increases with increasing deviation of the largest eigenvalue. Moreover, the distribution of the orientations of the principal eigenvectors in a region is consistent in the presence of anisotropic water diffusion. In the presence of isotropic diffusion, the orientations of the principal eigenvectors are random. The first aspect of diffusion anisotropy relates to the properties of a given VOI. The second aspect concerns the intervoxel relationships. Conventional diffusion anisotropy indices (FA and RA) focus on the first aspect only. Information concerning the eigenvectors of the diffusion tensor is purposely dismissed. On the other hand, IVDC quantifies the coherence of the directions of the principal diffusion tensor eigenvectors in a VOI and its nearest neighbors in 3D space. In contrast to other indices, the IVDC focuses on the second aspect of water diffusion. IVDC is calculated from the scatter matrix **T**, a second-order dyadic tensor developed from the principal eigenvectors of diffusion tensors. The index *raT* of the scatter matrix **T** has been shown to be sensitive to diffusion anisotropy. The IVDC may be regarded as a further development of *raT* that allows reconstruction of a quantitative whole-brain map that may be useful for diagnostic purposes.

Simulation Studies

FA and RA were used to characterize the extent of the anisotropy in white matter tracts. A digital phantom consisting of two fiber populations was used in our simulation studies. With separation between the fibers the orientation of the principal eigenvectors in both fiber populations

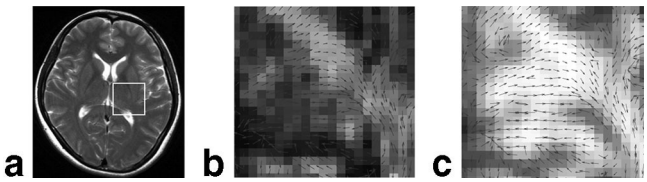

FIG. 4. FA and IVDC maps of the thalamus in a healthy volunteer. **(a)** T_2-weighted image. The box indicates the ROI. FA and IVDC were computed for each voxel in the ROI. The diffusion tensor eigenvector with the largest eigenvalue is projected onto the x-y plane. Arrows representing the projected principal eigenvector for each voxel in the ROI is superimposed onto the FA map **(b)** and onto the IVDC map **(c)**. The IVDC map demonstrates a homogeneous region of increased values where the principal eigenvectors are locally uniform. In contrast, the region demonstrates an inhomogeneous decrease in FA.

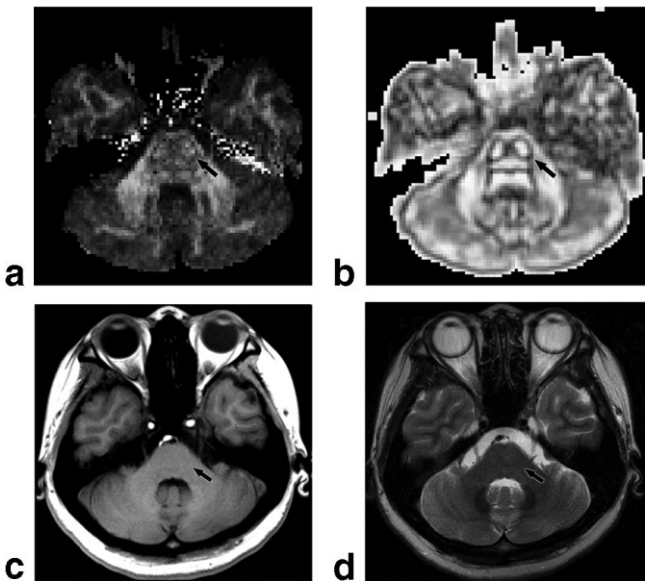

FIG. 5. FA and IVDC maps at the level of the middle cerebellar peduncles and pons. **(a)** Fractional Anisotropy, **(b)** InterVoxel Diffusion Coherence, **(c)** T_1-weighted image, and **(d)** T_2-weighted image.

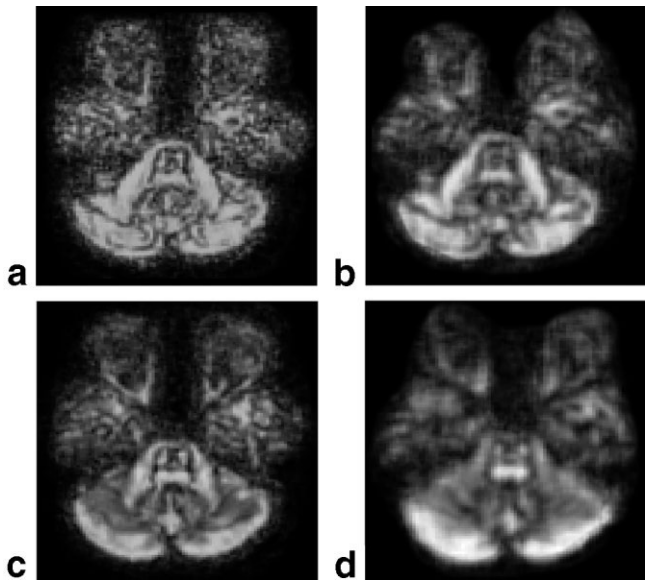

FIG. 6. IVDC maps derived from a different volunteer using different ROI sizes. Four different sizes were used. Distances from the original VOI were (3,3,1), (5,5,1), (3,3,3), and (5,5,5), respectively **(a–d)**.

changed continuously. The eigenvalues, however, remained unaffected by the separation of fiber populations since diffusivity does not necessarily change as the directions of diffusion change. As shown in Fig. 1, FA remained stable throughout the simulation, regardless of the orientation of the fiber populations. Because the eigenvalues were insensitive to these environmental variations, FA is not suitable for determining fiber tracking termination. In contrast, IVDC properly reflected coherence changes of the diffusion directions induced by the evolution of the fiber orientations. Figure 1 shows that IVDC decreased almost linearly with increasing separation angle. The decrease was close to linear between 25° and 65°.

The diffusion tensor model is inadequate in many circumstances, particularly in regions containing more than one coherently oriented fiber population (20–22). IVDC summarizes the information contained in the eigenvectors of the diffusion tensor in a 3D space. It has good properties for estimating separation between two fibers, even though diffusivity remains the same. On the other hand, CI failed to provide a systematic estimation of the diffusion coherence, which appeared to vary almost randomly within the range of the simulation.

Neither FA nor IVDC were affected by four different diffusion encoding schemes used in our study. IVDC is directly calculated from the principal eigenvectors of the diffusion tensor, and thus affected by the accuracy of the tensor reconstruction only. In contrast, CI varied greatly according to the diffusion encoding scheme, which cannot offer a consistent and reliable measure of diffusion anisotropy.

Reconstruction of Maps in Human Volunteers

The representative IVDC map shown in Fig. 2c demonstrates the feasibility of performing the computations on images acquired in vivo. In addition, IVDC maps provide similar image contrast in comparison to FA maps. IVDC was found to be increased in areas with unidirectional diffusion, as in white matter. IVDC is close to zero where the directions of diffusion are heterogeneous, as in the ventricles. The measured IVDC is consistent with *raT* reported by Wu et al. in selected ROI, as plotted in Fig. 3. The difference is significant in areas such as thalamus and splenium, which can be attributed to either different extent of partial volume contamination or difference in size of ROI.

The principal diffusion in fiber tracts was assumed to be dependent on the extent of myelination. Notably, measurements of the eigenvalues can be affected by noise during data acquisition, the diffusion encoding scheme, or other confounders. The magnitude of the principal eigenvalue can be altered. Conventional indices focusing on the relationship between eigenvalues might be easily affected by potential confounders. In this regard, a significant drop in FA was evident even in areas with uniform diffusion. On the other hand, the orientations of the eigenvectors may be preserved along the major direction of the fibers, even with a significant reduction of the principal eigenvalue within the same voxel. An index based on the calculation of the principal eigenvectors, as the IVDC, may therefore preserve the appropriate extent of diffusion anisotropy. Hence, it might properly reflect the extent of coherence of the directions of the principal diffusion.

CI is another eigenvector-based index. Although it provides a simple and straightforward approach, it did not allow easy anatomical identification of human brain structures. MR-based measurement of water diffusion is intrinsically bi-directional. The direction in the principal eigenvector can be reversed by the reversal of the third eigenvector. This phenomenon is frequently observed in areas of low signal-to-noise ratio. Under these circumstances, a negative cosine angle among the principal eigenvectors of the VOI and its neighborhoods occurs. The CI has been used previously to detect myelination and organization of the frontal white matter (14). However, the mean cosine angle may show a significant drop when the eigenvectors of two consecutive voxels are reversed. Specifically, CI may be drastically reduced or become negative. The reconstructed map is thus very noisy.

FA is calculated from the three eigenvalues in the VOI, which does not provide information on the diffusion between a voxel and its surrounding neighborhood. To overcome these limitations, FA maps are often color-encoded (Fig. 2b). It describes the directions of the principal eigenvectors qualitatively, thereby failing to provide a quantitative estimation of the diffusion anisotropy amongst different voxels.

The major disadvantage of IVDC is that it is computed from a mask of 26 surrounded voxels. Wu et al. (16) have previously shown that the *raT* can be affected by the number of voxels within the ROI. This is especially evident in areas where diffusion anisotropy is low. With the use of *raT*, a reduced size of ROI tends to overestimate the extent of diffusion anisotropy. This may result in areas of hyperintensity within the ventricle using the IVDC.

Application of the method to an ROI selected within the thalamus of a volunteer (Fig. 4) demonstrated that the projected principal diffusion tensor eigenvectors are lo-

cally homogeneous in orientation in this region, suggesting coherent fiber orientation. IVDC was consistently increased in regions where the direction of diffusion was uniform. In contrast, FA was decreased, implying a reduction in the coherence of the principal eigenvalues among the voxels of interest. This may be due to either a decreased longitudinal diffusivity or otherwise an increased noise variation during the measurement. Both these phenomena may lead to misdiagnosis. However, it should be noted that the relative fiber orientation among voxels remained unchanged even when the main eigenvalues decreased. IVDC thus provided an alternative and complementary method of estimating the diffusion coherence. Simulation studies showed that both FA and IVDC are not affected by diffusion encoding schemes under a noise-free condition.

Applied to the images acquired at the level of the pons (Fig. 5), the IVDC map reveals a clearly demarcated region of high values in each of the middle cerebellar peduncles. This finding likely reflects the highly organized structure and uniform fiber orientation of the middle cerebellar peduncles. This region is not as clearly delineated on the FA maps, demonstrating that IVDC maps may provide a superior image contrast for differentiating areas of varying fiber orientation characteristics. As would be expected, the corresponded T_1- and T_2-weighted images only provide a gross morphologic definition of the anatomic structures.

Another feature of the IVDC map is a clearly demarcated ring-like region of decreased IVDC on each side of the pons (Fig. 5b). These regions may indicate the sites where fiber tracts are crossing orthogonally. In contrast, the pons is homogeneous in signal intensity in the T_1- and T_2-weighted images (Fig. 5c,d). Although FA is decreased in these areas, the FA map appears more sensitive to degradation by noise and artifacts in comparison to the IVDC map. At these presumed sites where orthogonal fiber tracts cross, the IVDC is decreased to $\approx$0.56. This is in close agreement with the simulations, which resulted in an IVDC of 0.58 when the separation angle between the two fiber populations was 90° (Fig. 1). In comparison, the FA was constant and independent of the separation angle.

Coherence-based methods may lead to significant loss of resolution because the entire neighborhood effectively represents a low-resolution voxel. On the other hand, the IVDC method may have higher utility than FA in the presence of noise. Computation of IVDC relies on multiple voxels, thereby resulting in reduced noise secondary to an averaging effect. Wu et al. previously analyzed the effect of ROI size on *raT* computation by using Monte Carlo simulations. Their results showed that the *raT* tends to be overestimated for small ROI sizes, especially for more isotropic eigenvector distributions. Both the bias and variance of the estimated *raT* decrease if either the sample size is increased or the inherent *raT* is large.

Images from healthy volunteers were used to analyze the effect of different ROI sizes on the IVDC index. As shown in Fig. 6b,c for ROIs of similar size, this phenomenon may lead to a potential bias in the estimation of IVDC with the use of a 2D mask. Specifically, it should be noted that water diffusion in the through-plane direction is neglected. Images with a larger ROI size displayed an improved SNR, which is evident in Fig. 6d, where the ROI consisted of 124 voxels. The noise in the resultant IVDC map may be a combination of different factors including the size of the mask, inherent IVDC value, or the use of a 3D mask.

Using an ROI size of $3 \times 3 \times 3$, the spatial resolution is not significantly compromised compared to FA at a similar location. Moreover, diffusion coherence information between voxels may be maintained. The major disadvantage of using large ROIs is the image blurring which results from the smoothing effect, as is demonstrated in the areas near the middle cerebellar peduncle (Fig. 6). However, the use of a large local ROI may be feasible if different weightings are applied according to the relative distance from the VOI.

CONCLUSIONS

The InterVoxel Diffusion Coherence index may allow visualization of the coherence of the diffusion directions. It utilizes information contained in the eigenvectors of the diffusion tensor and may be calculated for a given VOI and its surroundings. It provides complementary information compared to the diffusion anisotropy as measured by FA. No additional data acquisition is required. Finally, IVDC may be useful in nerve fiber tractography, especially to determine the termination point of a trajectory.

REFERENCES

1. Filippi M, Inglese M. Overview of diffusion-weighted magnetic resonance studies in multiple sclerosis. J Neurol Sci 2001;186:S37–43.
2. Fu L, Matthews PM, De Stefano N, Worsley KJ, Narayanan S, Francis GS, Antel JP, Wolfson C, Arnold DL. Imaging axonal damage of normal-appearing white matter in multiple sclerosis. Brain 1998;121:103–113.
3. Warach S, Gaa J, Siewert B, Wielopolski P, Edelman RR. Acute human stroke studied by whole brain echo planar diffusion-weighted magnetic resonance imaging. Ann Neurol 1995;37:231–241.
4. Schocke MF, Seppi K, Esterhammer R, Kremser C, Mair KJ, Czermak BV, Jaschke W, Poewe W, Wenning GK. Trace of diffusion tensor differentiates the Parkinson variant of multiple system atrophy and Parkinson's disease. Neuroimage 2004;21:1443–1451.
5. Schocke MF, Seppi K, Esterhammer R, Kremser C, Jaschke W, Poewe W, Wenning GK. Diffusion-weighted MRI differentiates the Parkinson variant of multiple system atrophy from PD. Neurology 2002;58:575–580.
6. Pierpaoli C, Basser PJ. Toward a quantitative assessment of diffusion anisotropy. Magn Reson Med 1996;36:893–906.
7. Uluğ AM, van Zijl PC. Orientation-independent diffusion imaging without tensor diagonization: anisotropy definitions base on physical attributes of the diffusion ellipsoid. J Magn Reson Imaging 1999;9:804–813.
8. Basser PJ. Inferring microstructural features and the physiological state of tissues from diffusion weighted images. NMR Biomed 1995;8:333–344.
9. Hasan KM, Alexander AL, Narayana PA. Does fractional anisotropy have better noise immunity characteristics than relative anisotropy in diffusion tensor MRI? An analytical approach. Magn Reson Med 2004; 51:413–417.
10. Kingsley PB, Monahan WG. Contrast-to-noise ratios of diffusion anisotropy indices. Magn Reson Med 2005;53:911–918.
11. Wang JJ, Chao TC, Wai YY, Hsu YY. Novel diffusion anisotropy indices: an evaluation. J Magn Reson Imaging 2006;24:211–217.
12. Anderson AW. Theoretical analysis of the effects of noise on diffusion tensor imaging. Magn Reson Med 2001;46:1174–1188.
13. Basser PJ, Pierpaoli C. Microstuctural and physiological features of tissues elucidated by quantitative-diffusion-tensor MRI. J Magn Reson B 1996;111:209-219.
14. Klingberg T, Vaidya CJ, Gabrieli JD, Moseley ME, Hedehus M. Myelination and organization of the frontal white matter in children: a diffusion tensor MRI study. Neuroreport 1999;10:2817–2221.

15. Basser PJ, Pajevic S. Statistical artifacts in diffusion tensor MRI (DT-MRI) caused by background noise. Magn Reson Med 2000;44:41–50.
16. Wu YC, Field AS, Chung MK, Badie B, Alexander AL. Quantitative analysis of diffusion tensor orientation: theoretical framework. Magn Reson Med 2004;52:1146–1155.
17. Tournier JD, Calamente F, Gadian DG, Connely A. Direct estimation of the fiber orientation density function from diffusion-weighted MRI data using spherical deconvolution. Neuroimage 2004;23:1176–1185.
18. Jones DK, Horsfield MA, Simmons A. Optimal strategies for measuring diffusion in anisotropic systems by magnetic resonance imaging. Magn Reson Med 1999;42:515–525.
19. Jiang H, van Zijl PC, Kim J, Pearlson GD, Mori S. Dtistudio: resource program for diffusion tensor computation and fiber bundle tracking. Comput Methods Programs Biomed 2006;81:106–116.
20. Le Bihan D, Mangin JF, Poupon C, Clark CA, Pappata S, Molko N, Chabriat H. Diffusion tensor imaging: concepts and applications. J Magn Reson Imaging 2001;13:534–546.
21. Mori S, van Zijl PC. Fiber tracking: principles and strategies — a technical review. NMR Biomed 2002;15:468–480.
22. Wimberger DM, Roberts TP, Barkovich AJ, Prayer LM, Moseley ME, Kucharczyk J. Identification of "premyelination" by diffusion-weighted MRI. J Comput Assist Tomogr 1995;19:28–33.